



CHORUS

This is the accepted manuscript made available via CHORUS. The article has been published as:

Scaling between periodic Anderson and Kondo lattice models

R. Dong, J. Otsuki, and S. Y. Savrasov

Phys. Rev. B **87**, 155106 — Published 2 April 2013

DOI: [10.1103/PhysRevB.87.155106](https://doi.org/10.1103/PhysRevB.87.155106)

Scaling Between Periodic Anderson and Kondo Lattice Models

R. Dong¹, J. Otsuki^{2,3}, and S. Y. Savrasov¹

Department of Physics, University of California, Davis, California 95616, USA

²Department of Physics, Tohoku University, Sendai 980-8578, Japan

³Theoretical Physics III, Center for Electronic Correlations and Magnetism, Institute of Physics, University of Augsburg, D-86135 Augsburg, Germany

(Dated: February 19, 2013)

Continuous-Time Quantum Monte Carlo (CT-QMC) method combined with Dynamical Mean Field Theory (DMFT) is used to calculate both Periodic Anderson Model (PAM) and Kondo Lattice Model (KLM). Different parameter sets of both models are connected by the Schrieffer-Wolff transformation. For degeneracy $N = 2$, a special particle-hole symmetric case of PAM at half filling which always fixes one electron per impurity site is compared with the results of the KLM. We find a good mapping between PAM and KLM in the limit of large on-site Hubbard interaction U for different properties like self-energy, quasiparticle residue and susceptibility. This allows us to extract quasiparticle mass renormalizations for the f electrons directly from KLM. The method is further applied to higher degenerate case and to realistic heavy fermion system CeRhIn₅ in which the estimate of the Sommerfeld coefficient is proven to be close to the experimental value.

PACS numbers: 71.10.-w

I. INTRODUCTION

Computational study of heavy fermion materials¹ is a challenging theoretical problem. These systems are a subset of intermetallic compounds that have a low-temperature specific heat whose linear term is up to 1000 times larger than the value expected from the free-electron theory. The heavy fermion behavior has been found in rare earth and actinide metal compounds at very low temperatures (typically less than 10 K) in a broad variety of states including metallic, superconducting, insulating and magnetic states².

The physics of the heavy fermion systems is controlled by the antiferromagnetic interactions of local magnetic moments residing on the rare earth or actinide atoms with the sea of conduction electrons. The theoretical problem of a localized spin interacting with the conduction electrons is the celebrated Kondo problem³⁻⁸ whose solution is one of the outstanding achievements of many-body physics. It describes how the local spin is compensated as the temperature falls below a characteristic Kondo temperature. Something similar occurs in the heavy fermion materials which represents an array of such spins forming a Kondo lattice.

In this regime, each f orbital is occupied by a fixed number of electrons, and all types of charge fluctuations are approximately frozen due to a large Coulomb repulsion penalty that the system pays when the electron is added/removed from the shell. Therefore the low-energy degrees of freedom are provided by localized spins only and the corresponding model is known as the Kondo Lattice Model (KLM)⁹⁻¹⁷. The KLM effective Hamiltonian is obtained by using a second-order perturbation with respect to hybridization¹⁸ of a more general Periodic Anderson Model (PAM)¹⁹⁻²¹ where the localized f -electrons can exchange with the conduction electrons bath thus allowing both charge and spin fluctuations to occur. The

introduction of the limit of infinite dimensions and subsequent development of the dynamical mean field theory (DMFT) has allowed to study the properties of both models in a systematic manner²²⁻²⁸

Due to developments in the electronic structure theory for strongly correlated systems based on a combination of Density Functional Theory (DFT) in its local density approximation (LDA) and DMFT²⁹, studies of real heavy fermion materials have recently appeared in the literature³⁰⁻³². Here the development of Continuous Time Quantum Monte Carlo Method (CT-QMC) for solving corresponding Anderson Impurity problem has played a central role³³⁻³⁶. These calculations are extremely computationally demanding especially for the f elements such as Plutonium^{37,38} where a large number of atomic states needs to be kept in the calculation.

We have recently proposed a simplified approach³⁹ where instead of full solution of the Anderson impurity model, a corresponding Kondo Impurity (or more general Coqblin-Schrieffer Impurity⁴⁰) is studied to explore low-energy physics of heavy fermion materials^{41,42} using most recently developed CT-QMC algorithm for this problem⁴³⁻⁴⁵. In this regard, an interesting question arises on how exactly the scaling between Anderson and Kondo impurity models occurs and whether the low-energy properties of heavy fermion systems such as electronic mass enhancement and associated with it linear specific heat coefficient can be recovered from a restricted solution provided by the conduction electron self-energies available within the KLM. Such scaling behavior has been explored⁴⁶ for the temperature dependent susceptibility of the symmetric Anderson model using numerical renormalization group techniques⁷, where a precise mapping has been found to spin- $\frac{1}{2}$ Kondo Hamiltonian. Here we explore a similar mapping between single-particle functions such as the self-energy where upon increasing the value of on-site Coulomb repulsion U , we report a convergence of the conduction electron

self-energy extracted from the solution of the PAM to the one obtained within KLM. We use CT-QMC method for the corresponding impurity models and the Dynamical Mean Field Theory for achieving self-consistent solution of the lattice problem. We utilize an inverse relationship to extract the f -electron self-energies and monitor how the low-frequency behavior of the AIM converges to the KLM limit. Our obtained mapping allows the extraction of the mass renormalization of heavy quasiparticles directly from the solution of the Kondo lattice Hamiltonian.

As an illustration, we consider an electronic structure of CeRhIn₅ where we compute hybridization functions of the f -electrons with conduction bath and evaluate Kondo exchange coupling. We subsequently solve the Kondo Lattice Model with CT-QMC and DMFT, compute conduction electron self-energies, and then use the inverse mapping obtained from our analysis of the model Hamiltonian to evaluate electronic mass enhancement and specific heat coefficient of this system. Our theoretical results are compared with available experimental data.

This article is organized as follows. In Section II, we discuss the mapping between periodic Anderson model and Kondo lattice model in the limit of large U , and provide the results for electronic self-energies, quasiparticle residues and susceptibilities. In Section III, application is presented to evaluate electronic mass enhancement and Sommerfeld's coefficient for CeRhIn₅. Section IV is the conclusion.

II. MODEL CALCULATION

A. Periodic Anderson and Kondo Lattice Models

One of the popular models to describe the physics of heavy fermion materials is the periodic Anderson model¹⁹⁻²¹. The effective Hamiltonian is given by

$$H_{\text{PAM}} = \sum_{\mathbf{k}\sigma} \epsilon_{\mathbf{k}\sigma} c_{\mathbf{k}\sigma}^\dagger c_{\mathbf{k}\sigma} + \epsilon_f \sum_{i\sigma} f_{i\sigma}^\dagger f_{i\sigma} + U \sum_i n_{i\uparrow}^f n_{i\downarrow}^f + \sum_{i\mathbf{k}\sigma} V_{\mathbf{k}} (c_{\mathbf{k}\sigma}^\dagger f_{i\sigma} + H.c.) \quad (1)$$

where $c_{\mathbf{k}\sigma}^\dagger$ ($c_{\mathbf{k}\sigma}$) creates (destructs) a conduction electron with momentum \mathbf{k} , spin (and orbital) σ and dispersion $\epsilon_{\mathbf{k}\sigma}$; $f_{i\sigma}^\dagger$ ($f_{i\sigma}$) creates (destructs) an f electron with spin σ and energy ϵ_f on site i ; $n_{i\uparrow}^f$ ($n_{i\downarrow}^f$) is the number operator for f electron at lattice site i with spin up (down); U is the on-site Coulomb repulsion; $V_{\mathbf{k}}$ is the hybridization between f electrons and conduction electrons which we assume to be \mathbf{k} -independent, $V_{\mathbf{k}} = V$, for simplicity.

In systems where the Hubbard U is large, the charge fluctuations become effectively frozen and the ground state wave function has a little weight of configurations with the number of f -electrons different from its average number \bar{n}_f . This results in transforming the PAM

Hamiltonian which eliminates the hybridization term in the first order by Schrieffer-Wolff transformation. The second-order in V Hamiltonian is a famous Kondo Lattice Hamiltonian⁹⁻¹⁷ that describes interaction between spins of localized and conduction electrons

$$H_{\text{KLM}} = \sum_{\mathbf{k}\sigma} \epsilon_{\mathbf{k}\sigma} c_{\mathbf{k}\sigma}^\dagger c_{\mathbf{k}\sigma} + J_K \sum_i S_i \cdot \sigma \quad (2)$$

where S_i represents the localized spin of the f electron at the i site, the σ is the spin operator of the itinerant conduction electron and J_K is the Kondo coupling constant.

$$J_K = V^2 \left(\frac{1}{-\epsilon_f} + \frac{1}{\epsilon_f + U} \right). \quad (3)$$

For the half-filled case, $\epsilon_f = -U/2$, and J_K is simplified to $4V^2/U$.

B. Dynamical Mean Field Theory

Solutions of both models in a general case represent a complicated numerical problem. Using dynamical mean field theory, the algorithm breaks down into (i) the solution of the corresponding (Anderson or Kondo) impurity problem and (ii) the self-consistency loop over hybridization functions which enforces lattice periodicity²⁵.

For the periodic Anderson model, the DMFT evaluates the local Green function for heavy electrons

$$G_f^{(loc)}(i\omega_n) = \sum_{\mathbf{k}} \left[i\omega_n - \epsilon_f - \Sigma_f(i\omega_n) - \frac{V^2}{i\omega_n - \epsilon_{\mathbf{k}}} \right]^{-1}.$$

Then, the bath Green function is defined

$$G_f^{(0)-1}(i\omega_n) = G_f^{-1}(i\omega_n) + \Sigma_f(i\omega_n) \equiv i\omega_n - \epsilon_f - \Delta(i\omega_n)$$

and used as an input to the impurity solver. The latter produces an impurity Green function

$$G_f^{(imp)}(i\omega_n) = \frac{1}{i\omega_n - \epsilon_f - \Delta(i\omega_n) - \Sigma_f(i\omega_n)}$$

from where, a new self-energy can be found

$$\Sigma_f(i\omega_n) = G_0^{-1}(i\omega_n) - G_f^{(imp)-1}(i\omega_n).$$

The process is repeated by recalculating the lattice Green function with the new self-energy. The self-consistency condition is when

$$G_f^{(imp)}(i\omega_n) = G_f^{(loc)}(i\omega_n).$$

The Kondo lattice Hamiltonian can be obtained by considering the limit $V^2 \rightarrow \infty, U \rightarrow \infty, \epsilon_f \rightarrow -\infty$ while keeping $V^2/\epsilon_f = \text{const}$. First, define a local Green function for conduction electrons

$$G_c^{(loc)}(i\omega_n) = \sum_{\mathbf{k}} [i\omega_n - \epsilon_{\mathbf{k}} - \Sigma_c(i\omega_n)]^{-1}$$

where conduction electron self energy is given by

$$\Sigma_c(i\omega_n) = \frac{V^2}{i\omega_n - \epsilon_f - \Sigma_f(i\omega_n)}.$$

Thus, in the DMFT self-consistent loop one can iterate over conduction electron quantities: The bath Green function

$$G_c^{(0)-1}(i\omega_n) = G_c^{(loc)-1}(i\omega_n) + \Sigma_c(i\omega_n)$$

serves as the input to the Kondo impurity solver. The latter produces an impurity Green function $G_c^{(imp)}(i\omega_n)$ from which the new conduction electron self-energy is found. The process is repeated by reevaluating $G_c^{(loc)}(i\omega_n)$. The self-consistency condition is when

$$G_c^{(imp)}(i\omega_n) = G_c^{(loc)}(i\omega_n).$$

Several powerful methods such as exact diagonalization or numerical renormalization group techniques have been developed in the past to deal with the impurity models. In this work we utilize a Continuous Time Quantum Monte Carlo method^{33–36} that was originally proposed to deal with Anderson impurities but has been recently generalized for Kondo (Coqblin–Schrieffer) type of impurities⁴³.

The density of states of conduction electrons is an input to the simulation. Despite realistic materials may have complex band structures, we use a simple constant density of states to gain the physical insight from these calculations. The half-bandwidth D is set to 1 which provides the corresponding units. As we are looking for a mapping between the two models in the regime of large U , we first fix the Kondo coupling J_K to some predetermined value. There are typically two phases that emerge in the KLM: the antiferromagnetic RKKY phase and the paramagnetic Fermi liquid phase, which compete with each other on the scale of J_K ¹¹. We are mainly interested in the Fermi liquid behavior and consider the value of $J_K = 0.3$ in all our calculations. Second, we study two cases with the effective f-electron degeneracies $N = 2$ and $N = 4$. For the case $N = 2$, the only non-trivial occupancy of the f-orbital is 1 which for the particle-hole symmetric placement of the conduction electron band results in the condition $\epsilon_f = -U/2$, for the f orbital to be half-filled. Although the system becomes a band (Kondo) insulator in this case, the f-electrons states are strongly renormalized by correlations which is the basis for the comparison of these two models.

C. DMFT Solutions for $N = 2$

We first discuss the solutions for the case $N = 2$. The behavior of density of f-electron states obtained from the solution of the periodic Anderson model for several values of Hubbard $U = 3, 6, 9$ using CT QMC algorithm at

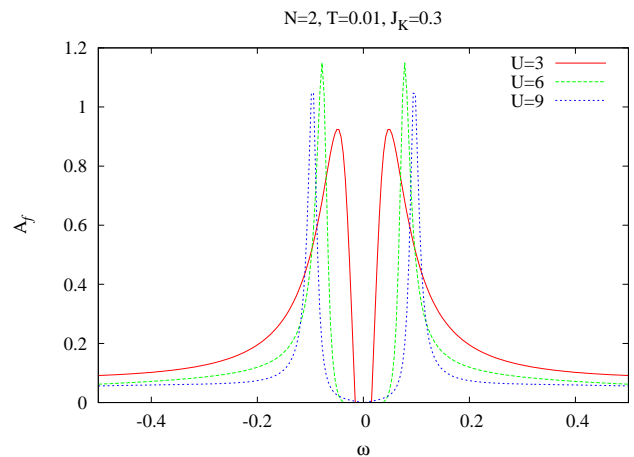


FIG. 1: (color online) Density of f-electron states obtained from the solution of the periodic Anderson model for the values of Hubbard $U = 3, 6, 9$.

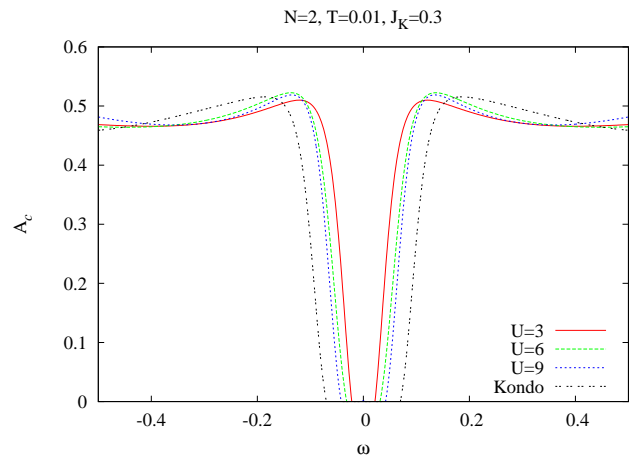


FIG. 2: (color online) Conduction electron density of states obtained from the solution of the periodic Anderson model for the values of Hubbard $U = 3, 6, 9$. Also shown the result obtained from the Kondo lattice simulation.

imaginary axis and analytically continued to the real frequencies is shown in Fig. 1. We can see that the energy gap is opened up at the Fermi level as we expected. As U increases, the peaks get narrower which correspond to smaller values of quasiparticle residue z_f . Since we fix $J_K = 4V^2/U$, the hybridization increases according to U and so does the hybridization gap.

The behavior of the conduction electron density of states from the PAM calculation is shown in Fig. 2 where we also see the gap that gets opened at the Fermi energy. The result of the simulation using the Kondo lattice model is shown here as well for comparison. Upon increasing U , we see that the conduction electron DOS of the PAM tends to the infinite U limit represented by the KLM calculation.

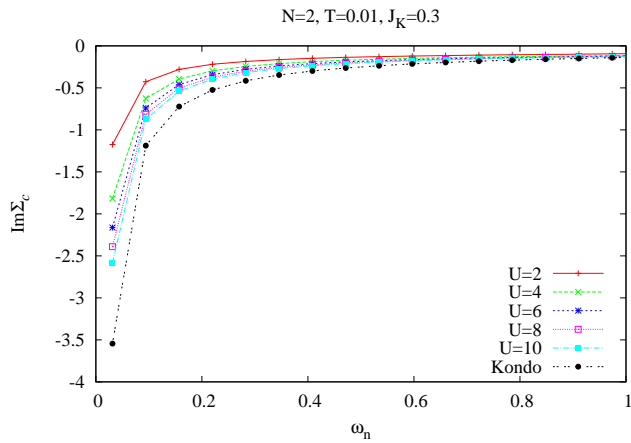


FIG. 3: (color online) Conduction electron self-energy of the periodic Anderson model with $N = 2$ calculated for several values of U and the conduction electron self-energy of the Kondo lattice model that corresponds to $U \rightarrow \infty$ limit.

1. Self-energies

We first obtain the f-electron self-energy from the PAM calculation. Then we extract the conduction electron self-energy and compare with the data of the KLM simulation. We present such comparison in Fig. 3 where we plot $\Im\Sigma_c(i\omega_n)$ for several values of U and $U \rightarrow \infty$ limit corresponding to KLM. We monitor a slow convergence of the PAM self-energy towards its KLM value, although even for $U = 10$ the discrepancy between the two is still noticeable.

We now address the question of $U \rightarrow \infty$ limit for the f-electron self-energies, which numerically corresponds to the Kondo regime, and compare these data with our scaling behavior established analytically. First, notice that the low-frequency expansion for both f-electron and conduction electron quantities can be derived without a problem

$$\Sigma_{f,c}(i\omega_n) = \Sigma_{f,c}(0) + i\omega_n(1 - z_{f,c}^{-1})$$

which leads us to

$$\begin{aligned} \Sigma_f(0) &= -\epsilon_f - \frac{V^2}{\Sigma_c(0)} \\ z_f &= \frac{[\Re\Sigma_c(0)]^2}{V^2} \frac{z_c}{1 - z_c}. \end{aligned} \quad (4)$$

This formula has been used in our recent LDA+DMFT work to extract mass renormalization parameters in several heavy fermion compounds⁴² using simulations with the Kondo lattice.

Unfortunately, this approach will not work for the model considered here since for the particle-hole symmetric case of the Kondo insulator, the conduction electron self-energies diverge to produce an energy gap in

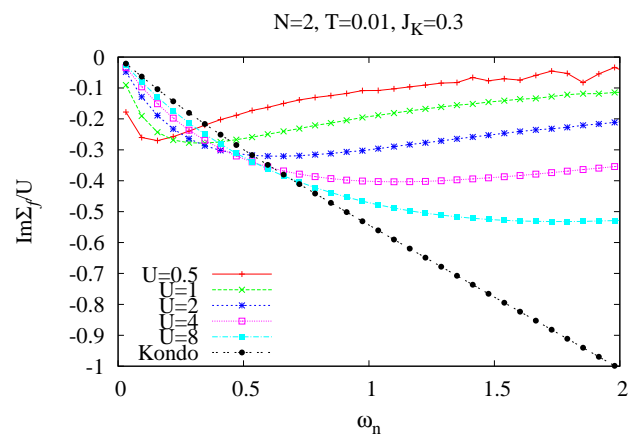


FIG. 4: (color online) The convergence for the f-electron self-energy obtained from the periodic Anderson model with $N = 2$ upon increase in the interaction U . The limiting behavior of this quantity extracted from the solution of the Kondo lattice model is also plotted.

the excitation spectrum. We therefore look for a scaling behavior in a different way. We write

$$\Sigma_f(i\omega_n) = i\omega_n - \epsilon_f - \frac{V^2}{\Sigma_c(i\omega_n)} \quad (5)$$

and noticing that we target the $U \rightarrow \infty$ limit, we replace V^2 with $\frac{1}{4}J_K U$, and divide both parts by U . For the imaginary part we obtain the following scaling behavior

$$\frac{\Im\Sigma_f(i\omega_n)}{U} = \frac{J_K \Im\Sigma_c(i\omega_n)}{4|\Sigma_c(i\omega_n)|^2} \quad (6)$$

that expresses the large U limit of the PAM self-energy via the quantities available within KLM.

The self-energies from both models can now be directly compared. Fig. 4 shows the behavior of $\Im\Sigma_f(i\omega_n)/U$ for several values of U together with the corresponding data extracted from KLM. From the figure we see that as U increases the PAM self-energy converges to that of the KLM. The plot actually includes both the intermediate regime and the Kondo regime. When $U < 2$ the two Hubbard bands are within the conduction electron band which has a bandwidth of 2 in our units. In this case the self-energy deviates more than the data for $U \geq 2$. As U goes to 8, the self-energies from both models collapse at low energies.

Finally, we notice here that the $U \rightarrow \infty$ limit produces $\Im\Sigma_f(i\omega_n)/U$ that grows linearly with the frequency which is exactly the case of the self-energies obtained in slave-boson type of methods for solving the impurity problems^{47,48} or within quasiparticle Gutzwiller approximation⁴⁹.

2. Quasiparticle Residues

Our self-energy results show qualitative convergence between the two models. To get quantitative agreement we further check the quasiparticle residues that we extract from the low frequency behavior of the self-energies. These are related to renormalized effective masses for the quasiparticles responsible for the enhanced specific heat coefficient which is one of the central properties of systems with heavy fermions.

The CT-QMC algorithm works on an imaginary time axis, which after the Fourier transformation gives us the data on the imaginary frequency axis. Analytically continued to the real axis, the real part of the self-energy around the Fermi level exhibits a linear behavior with the slope determining the electronic mass enhancement, while its imaginary part exhibits a quadratic behavior which is a known result of the Fermi liquid theory. Despite problems associated with numerical noise that prevents us to extract accurate data at real frequencies using analytical continuation, we can find the quasiparticle residue from the imaginary axis data as follows:

$$z = \left(1 - \frac{\partial \Im \Sigma(i\omega_n)}{\partial (i\omega_n)} \Big|_{\omega_n \rightarrow 0}\right)^{-1}. \quad (7)$$

For the KLM, according to Eq. (5), the z_f can be written as:

$$z_f^{KLM} = -\frac{4\pi T |\Sigma_c(i\pi T)|^2}{J_K U \Im \Sigma_c(i\pi T)}. \quad (8)$$

Although this expression is actually valid only for $U = \infty$, where z_f^{KLM} becomes zero, we expect that it gives an approximate value for PAM with $U < \infty$.

We present our comparisons between the two quantities in Fig. 5 where we plot the quasiparticle residue extracted from PAM as a function of U as well as the one extracted from the KLM according to Eq. (8). Also plotted for comparison is the quasiparticle residue calculated using the slave-boson method as described in Ref. 48.

From the plots, we can quantitatively see the convergence from the result obtained from PAM to the one obtained by KLM. When U reaches 10, the KLM overestimates z_f of the PAM data by about 30%. While the slave-boson method, a very fast calculation, demonstrates a similar behavior, it overestimates the PAM data by about 100%.

3. Susceptibilities

Since the KLM freezes the spatial fluctuations but keeps the essential magnetic properties, the corresponding spin susceptibilities $\chi(T)$ should agree between the

FIG. 5: (color online) Comparison between quasiparticle residues z_f calculated as a function of Hubbard U using periodic Anderson model with $N = 2$, Kondo lattice model as well as a slave-boson method described in Ref. 48.

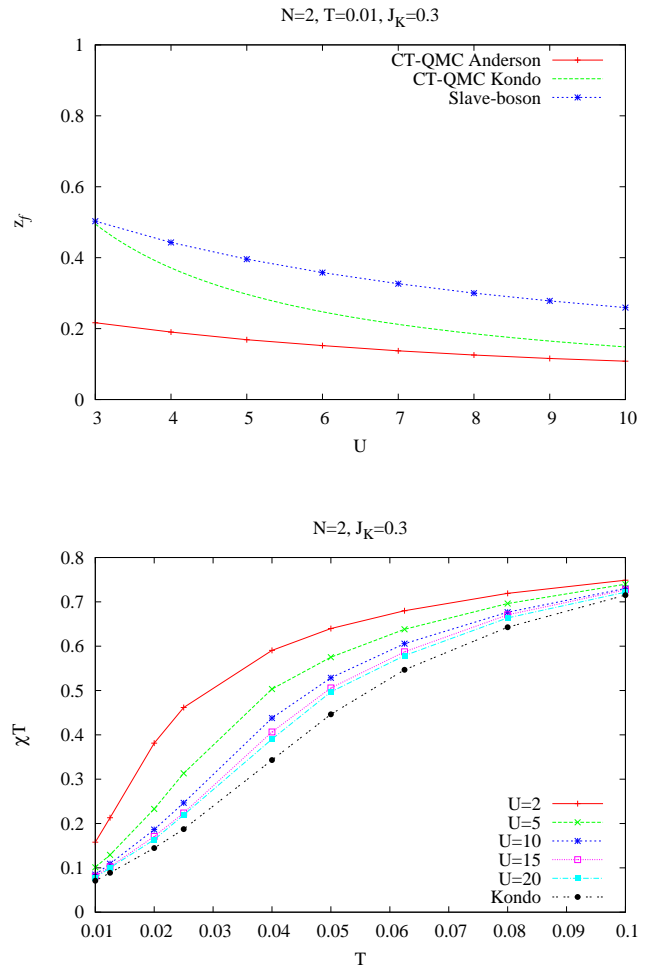


FIG. 6: (color online) Calculated using the periodic Anderson model with $N = 2$ temperature dependence of spin susceptibility (times the temperature) for several values of Hubbard U as well as the data extracted for the Kondo lattice model.

PAM and KLM at least for low temperatures. Indeed, these quantities have been calculated and compared against each other for the corresponding impurity models using numerical renormalization group methods long time ago⁴⁶ where a precise mapping between Anderson impurity and spin- $\frac{1}{2}$ Kondo impurity has been observed.

We present our own calculations in Fig. 6 where we plot $T\chi(T)$ against the temperature for several values of U calculated using the PAM as well as the data extracted from the KLM. The comparison shows a nice convergence for susceptibility within our chosen temperature range. The deviation may result from the combination of thermal effect and charge fluctuations. We see that the convergence is worse here than that for the quasiparticle

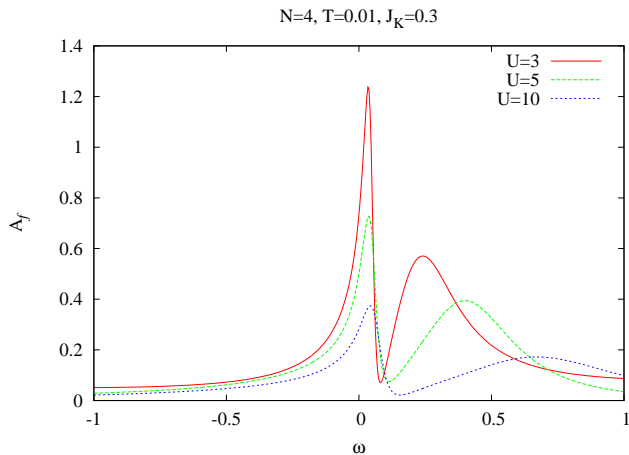


FIG. 7: (color online) Density of f-electron states obtained from the solution of the periodic Anderson model for the values of Hubbard $U = 3, 5, 10$.

residues discussed earlier, but we believe that the susceptibilities should map precisely to each other at lower temperatures.

D. DMFT Solutions for $N = 4$

The $N = 2$ case with one localized electron leads to the Kondo insulator state which is topologically special. However, our method can be generalized to larger orbital degeneracy, where any integer occupancy of the f-shell can be explored. Also the Coqblin-Schrieffer model is more favorable. Below we consider the case with $N = 4$ and $n_f = 1$ which is away from particle-hole symmetry. As is the case with $N = 2$, we fix the value of the Kondo coupling J_K to 0.3. For each value of U that we input to the PAM calculation, there are two remaining parameters, the impurity level ϵ_f , and the value of hybridization V^2 that should be searched for to obtain $n_f = 1$, $J_K = 0.3$.

The density of f-electron states obtained from the solution of the periodic Anderson model for several values of Hubbard $U = 3, 5, 10$ is shown in Fig. 7. Away from particle-hole symmetry, this shows a Fermi-liquid behavior, i.e. a quasiparticle peak at the Fermi level instead of the hybridization gap. As U increases, the trend is similar to the $N = 2$ case, Fig. 1.

The behavior of the conduction electron density of states from the PAM calculation is shown in Fig. 8, together with the result of the simulation using the Kondo lattice model. Upon increasing U , the conduction electron DOS of the PAM tends to the infinite U limit given by the Kondo lattice.

Conduction electron self-energies $\Im\Sigma_c(i\omega_n)$ calculated within PAM for several values of U as well as within KLM corresponding to $U \rightarrow \infty$ limit are compared in Fig. 9. We see that the convergency of $\Im\Sigma_c(i\omega_n)$ is rather slow

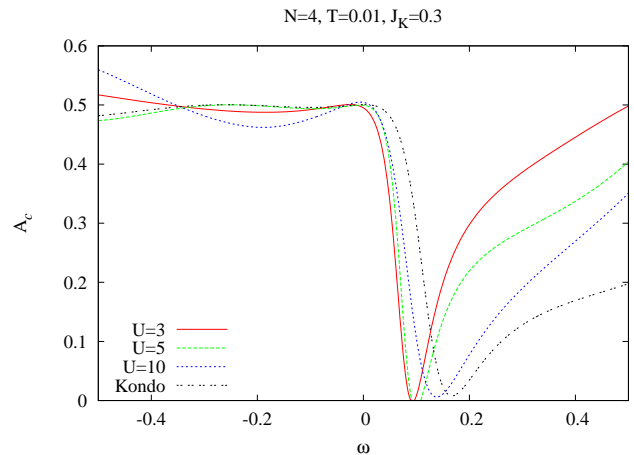


FIG. 8: (color online) Conduction electron density of states obtained from the solution of the periodic Anderson model for the values of Hubbard $U = 3, 5, 10$. Also shown is the result of the simulation with the Kondo lattice.

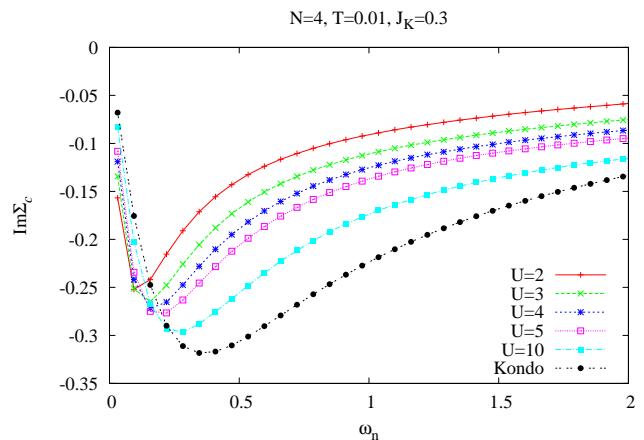


FIG. 9: (color online) Conduction electron self-energy of the periodic Anderson model with $N = 4$ calculated for several values of U and the conduction electron self-energy of the Kondo lattice model that corresponds to $U \rightarrow \infty$ limit.

when U increases similar to the $N = 2$ case presented in Fig. 3. The low frequency behavior of $\Im\Sigma_c(i\omega_n)$ shows that the hybridization gap is no longer opened at the Fermi energy and the system remains metallic contrary to the particle-hole symmetric case of the Kondo insulator where $\Im\Sigma_c(i\omega_n)$ diverges at $i\omega_n \rightarrow 0$ as seen on Fig. 3. Here, the low-frequency slopes determine quasiparticle residues z_c for conduction electrons which display a somewhat faster convergence to the Kondo limit upon increase in U .

To compare how $\Sigma_f(i\omega_n)$ scales to the Kondo limit, we start from Eq. (5), take its imaginary part and divide by U on both sides. Using Eq. (3), the formula becomes:

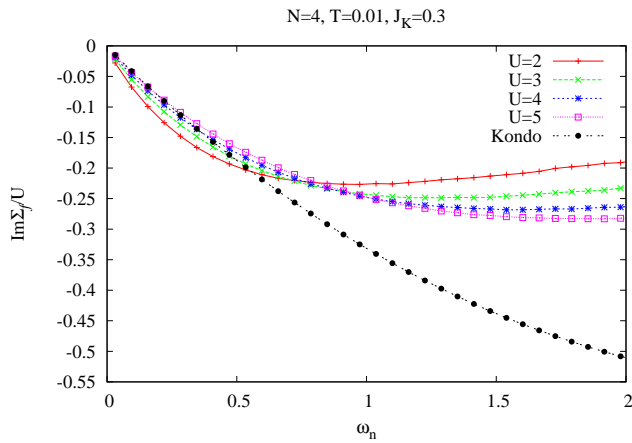


FIG. 10: (color online) The convergence for the f–electron self–energy obtained from the periodic Anderson model with $N = 4$ upon increase in the interaction U . The limiting behavior of this quantity extracted from the solution of the Kondo lattice model is also plotted.

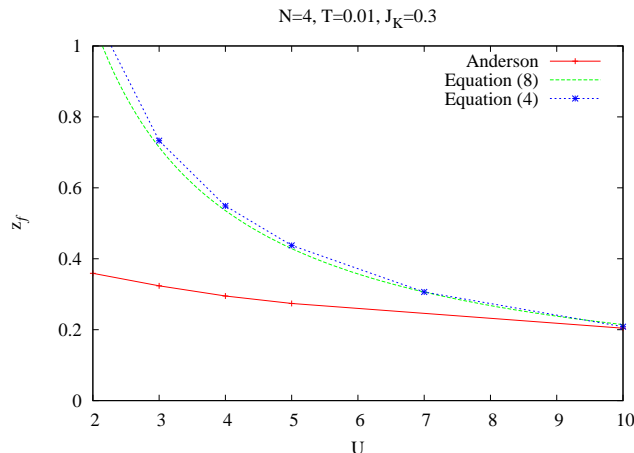


FIG. 11: (color online) Comparison between quasiparticle residues z_f calculated as a function of Hubbard U using periodic Anderson model with $N = 4$, and the values extracted from the Kondo lattice model using two different approaches described in text.

$$\frac{\Im\Sigma_f(i\omega_n)}{U} = \frac{i\omega_n}{U} + J_K\eta(1-\eta)\frac{\Im\Sigma_c(i\omega_n)}{|\Sigma_c(i\omega_n)|^2} \quad (9)$$

where $\eta = -\frac{\epsilon_f}{U}$ is a dimensionless parameter which affects the electron counting at impurity site.

Fig. (10) presents the behavior of $\Im\Sigma_f(i\omega_n)/U$ calculated within PAM for several values of U together with the corresponding data extracted from KLM. From the figure we see that as U increases, the PAM self–energy maps into its $U \rightarrow \infty$ limit of the KLM.

The low–frequency behavior of $\Im\Sigma_c(i\omega_n)$ shown in Fig. 9 may lead to a conclusion on the presence of

some exotic non–Fermi liquid behavior but this is actually only a temperature effect. Our model with $N = 4$ (Coqblin–Schrieffer model and multiorbital periodic Anderson model) has the ordinary Kondo fixed point and does not show undercompensated or two–channel Kondo effect. Indeed, the f–electron self–energy in Fig. 10 clearly shows a Fermi–liquid behavior

We have finally extracted the values for quasiparticle residues from the low–frequency slopes of $\Im\Sigma_f(i\omega_n)$ which can be compared with the values of z_f that we obtain from the KLM calculation either using the approach that leads us to Eq.(8) or using the low–frequency behavior of $\Im\Sigma_c(i\omega_n)$ that leads us to Eq. (4). We present such comparison in Fig. 11 where the behavior of z_f is plotted against Hubbard U . We see that starting from $U = 10$, the quasiparticle residues computed from PAM and KLM become very close to each other.

III. APPLICATION TO CeRhIn₅

Realistic heavy fermion materials have much more complicated electronic structures than we used in our model calculations. The f–orbitals are 14–fold degenerate and split in the presence of spin–orbit coupling and crystal–field effects. This makes LDA+DMFT calculations with full solution of Anderson impurity problem dramatically heavy. With the advantage of reaching lower temperature range, LDA+DMFT simulations with Kondo (or Coqblin–Schrieffer) impurity was established³⁹. In this method, the first step is to find the local hybridization function $\Delta_\alpha(\epsilon)$ between fully localized f and conduction spd electrons, where subscript α refers to a particular representation that tries to diagonalize a general matrix $\Delta_{m'\sigma'm\sigma}(\epsilon)$ by taking advantage of spin–orbit and crystal–field symmetries. This is achieved by using the so called Hubbard I approximation⁵⁰ where purely atomic f–electron self–energy is entered to the LDA+DMFT calculation. Knowing $\Delta_\alpha(\epsilon)$, the Kondo coupling constant J_K and the initial Green’s function of conduction electrons can be extracted.

$$G_\alpha(i\omega_n) = \int_{-D_{\text{cutoff}}}^{D_{\text{cutoff}}} d\epsilon \frac{\Im\Delta_\alpha(\epsilon)}{i\omega_n - \epsilon} / \int_{-D_{\text{cutoff}}}^{D_{\text{cutoff}}} d\epsilon \Im\Delta_\alpha(\epsilon), \quad (10)$$

and

$$V_\alpha^2 = \frac{1}{\pi} \int_{-D_{\text{cutoff}}}^{D_{\text{cutoff}}} d\epsilon \frac{\Im\Delta_\alpha(\epsilon)}{N_F}. \quad (11)$$

These are required for solving realistic Kondo lattice problem with J_K calculated from the Schrieffer–Wolff transformation, Eq. (3).

Our target material is CeRhIn₅ which is believed to have the most localized f–electrons in the 115 family. The spin–orbit coupling and crystal fields of the tetragonal structure effectively reduce the degeneracy and make the Γ_7 doublet of the $j = 5/2$ state to be the ground state.

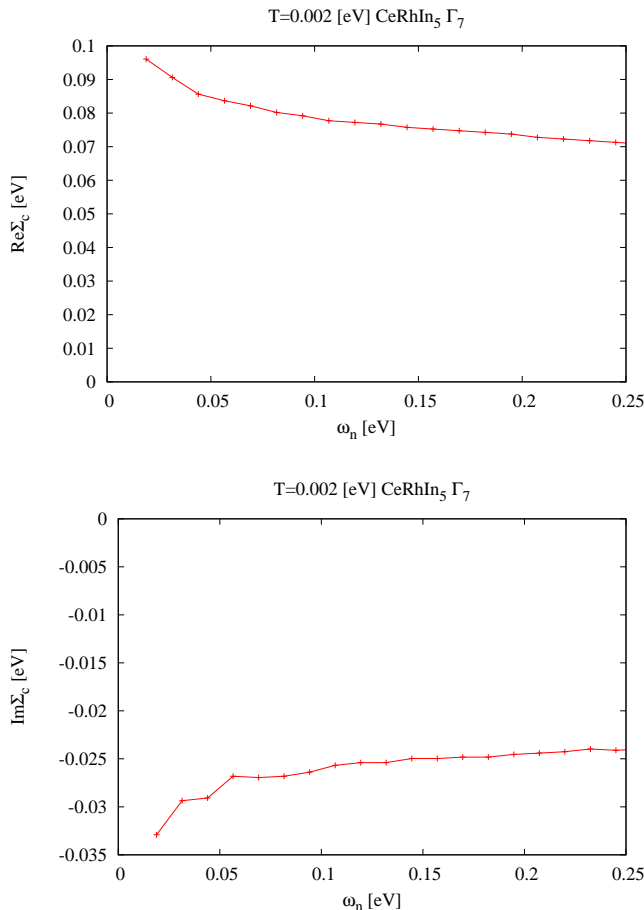


FIG. 12: (color online) Conduction electron self-energies $\Re\Sigma_c(\epsilon)$ (top plot) and $\Im\Sigma_c(\epsilon)$ (bottom plot) of Γ_7 states for CeRhIn₅ at temperature $T = 0.002$ eV (≈ 23 K) calculated using the LDA+DMFT method with the Kondo lattice.

TABLE I: Calculated LDA density of states at the Fermi energy, $N(0)$ (states/eV/cell), the hybridization V^2 (eV²), estimated quasiparticle residue z_f for the f-electrons as well as predicted and experimental values of the Sommerfeld coefficient γ (mJ/mol/K²) for CeRhIn₅.

materials	$N(0)_{\text{LDA}}$	V^2	z_f	γ	γ_{exp}
CeRhIn ₅	2.21	0.16	0.01255	414	400 ^a

^aRef.51

Therefore at very low temperatures, a single localized f-electron resides at the Γ_7 doublet and we have the $N = 2$ case discussed above in the model calculation.

A general LDA+DMFT calculation for this material has been done in the former work³⁹ with $\epsilon_f = -2.5$ eV and $U = 5$ eV which are the typical values for Ce-based compounds. Here we provide an analysis of its low energy physical properties. Fig. 12 shows calculated conduction electron self-energies, $\Re\Sigma_c(\epsilon)$ and $\Im\Sigma_c(\epsilon)$, for the Γ_7 state from our LDA+DMFT simulation with the Kondo lattice. We clearly see that the imaginary part of Σ_c

tends to diverge at least to $T \approx 23$ K although this behavior could result from the temperature being not low enough in our simulation. However, a conventional low-frequency expansion of the self-energy and the connection between z_f and z_c , Eq. (4), cannot be utilized to estimate the quasiparticle residue for the f electrons and the Sommerfeld coefficient γ .

Here we use our mapping method to extract z_f exactly as we illustrated for our model calculation. In this way, we first estimate the quasiparticle residue z_f and, second, evaluate the renormalized density of states at the Fermi level $N(0)_{\text{eff}} = N(0)_{\text{LDA}}/z_f$. Then the Sommerfeld coefficient can be found

$$\gamma = \frac{1}{3}\pi N_{\text{eff}}(0). \quad (12)$$

All calculated properties are summarized in Table I. It can be seen that our estimate for γ is very close to the experimental value which indicates that our simulation is sufficiently accurate to describe this material.

IV. CONCLUSION

We have studied a mapping of periodic Anderson model to the Kondo lattice model in the limit of $U \rightarrow \infty$ for single-particle functions such as the self-energy. The crossover occurs at the values of interaction $U = 10D$ where the models become equivalent. This allowed us to map the quasiparticle residue z_f of the f-electrons and extract its values directly from the Kondo lattice model. We applied the method to realistic heavy fermion system CeRhIn₅ where our estimates for the Sommerfeld coefficient agree well with the experiment.

ACKNOWLEDGMENTS

We gratefully acknowledge useful discussions with X. G. Wan and Shu-Ting Pi. The work was supported by DOE NEUP under Contract No. 00088708.

-
- ¹ For a review, see, e.g., G. R. Stewart, Heavy fermion systems, *Reviews of Modern Physics* **56**, 755 (1984).
- ² For a review, see, e.g., Heavy Fermion Systems, ed. by P. Misra (Elsevier, 2007).
- ³ J. Kondo, *Progr. Theor. Phys. Osaka*, 32, 37 (1964).
- ⁴ A. Abrikosov, *Physics* **2**, 5 (1965).
- ⁵ H. Suhl, *Phys. Rev.* **138**, A515 (1965).
- ⁶ Y. Nagaoka, *Phys. Rev.* **138**, A1112 (1965).
- ⁷ K. G. Willson, *Rev. Mod. Phys.* **47**, 773 (1975).
- ⁸ For a review, see, e.g., A. C. Hewson, *The Kondo Problem to Heavy Fermions*, Cambridge University Press, 1995.
- ⁹ C. Lacroix and M. Cyrot, *Phys. Rev. B* **20**, 1969 (1979).
- ¹⁰ P. Coleman, N. Andrei, *J. Phys., Condens. Matter* **1**, 4057 (1989).
- ¹¹ S. Doniach, *Phys. Rev. B* **35**, 1814 (1987).
- ¹² S. Caprara and A. Rosengren, *Europhys. Lett.* **39**, 55 (1997).
- ¹³ H. Tsunetsugu, M. Sigrist, K. Ueda, *Rev. Mod. Phys.* **69**, 809 (1997).
- ¹⁴ M. Lavagna, C. Pépin, *Acta Physica Polonica B* **29**, 3753 (1998).
- ¹⁵ Q. Si, S. Rabello, K. Ingersent and J. L. Smith, *Nature* **413**, 804 (2001).
- ¹⁶ W. Nolting, G. G. Reddy, A. Ramakanth, D. Meyer, and J. Kienert, *Phys. Rev. B* **67**, 024426 (2003).
- ¹⁷ T. Senthil, S. Sachdev, and M. Vojta, *Phys. Rev. Lett.* **90**, 216403 (2003).
- ¹⁸ J. R. Schrieffer and P. A. Wolff, *Phys. Rev.* **149**, 491 (1966).
- ¹⁹ S.R. Jullian and R. M. Martin, *Phys. Rev. B* **26**, 6173 (1982).
- ²⁰ T. M. Rice, K. Ueda, *Phys. Rev. Lett.* **55**, 995 (1985).
- ²¹ R. Blankenbecler, J. R. Fulco and W. Gill, D. J. Scalapino, *Phys. Rev. Lett.* **58**, 411 (1987).
- ²² W. Metzner and D. Vollhardt, *Phys. Rev. Lett.* **62**, 324 (1989).
- ²³ A. Georges and G. Kotliar, *Phys. Rev. B* **45**, 6479 (1992).
- ²⁴ M. Jarrell, *Phys. Rev. Lett.* **69**, 168 (1992).
- ²⁵ For a review, see, A. Georges, G. Kotliar, W. Krauth, and M. Rozenberg, *Rev. Mod. Phys.* **68**, 13 (1996).
- ²⁶ M. Jarrell, H. Akhlaghpour, Th. Pruschke, *Phys. Rev. Lett.* **70**, 1670 (1993).
- ²⁷ Th. Pruschke, R. Bulla, M. Jarrell, *Phys. Rev. B* **61**, 12799 (2000).
- ²⁸ N. Matsumoto and F. J. Ohkawa, *Phys. Rev. B* **51**, 4110 (1995).
- ²⁹ G. Kotliar, S. Savrasov, K. Haule, V. Oudovenko, O. Parcollet, and C. Marianetti, *Rev. Mod. Phys.* **78**, 865 (2006).
- ³⁰ K. Held, A.K. McMahan, R.T. Scalettar, *Phys. Rev. Lett.* **87**, 276404 (2001).
- ³¹ K. Haule, V. Oudovenko, S. Y. Savrasov, G. Kotliar, *Phys. Rev. Lett.* **94**, 036401 (2005).
- ³² J. H. Shim, K. Haule and G. Kotliar, *Science* **318**, 1615 (2007).
- ³³ A. N. Rubtsov, V. V. Savkin, and A. I. Lichtenstein, *Phys. Rev. B* **72**, 035122 (2005).
- ³⁴ P. Werner, A. Comanac, L. de' Medici, M. Troyer, and A. J. Millis, *Phys. Rev. Lett.* **97**, 076405 (2006).
- ³⁵ K. Haule, *Phys. Rev. B* **75**, 155113 (2007).
- ³⁶ For a review, see, E. Gull, A.J. Millis, A. I. Lichtenstein, A. N. Rubtsov, M. Troyer, and P. Werner, *Rev. Mod. Phys.* **83**, 349 (2011).
- ³⁷ J. H. Shim, K. Haule, S. Savrasov, and G. Kotliar, *Phys. Rev. Lett.* **101**, 126403 (2008).
- ³⁸ J. H. Shim, K. Haule, and G. Kotliar, *Nature* **446**, 513 (2007).
- ³⁹ M. Matsumoto, M. J. Han, J. Otsuki, S. Y. Savrasov, *Phys. Rev. Lett.* **103**, 096403 (2009).
- ⁴⁰ B. Coqblin and J. R. Schrieffer, *Phys. Rev.* **185**, 847 (1969).
- ⁴¹ M. Matsumoto, M. J. Han, J. Otsuki, S. Y. Savrasov, *Phys. Rev. B* **82**, 180515 (2010).
- ⁴² M. Matsumoto, Q. Yin, J. Otsuki, S. Y. Savrasov, *Phys. Rev. B* **84**, 041105 (2011).
- ⁴³ J. Otsuki, H. Kusunose, P. Werner, and Y. Kuramoto, *J. Phys. Soc. Jpn.* **76**, 114707 (2007).
- ⁴⁴ J. Otsuki, H. Kusunose, and Y. Kuramoto, *J. Phys. Soc. Jpn.* **78**, 014702 (2009).
- ⁴⁵ J. Otsuki, H. Kusunose, and Y. Kuramoto, *Phys. Rev. Lett.* **102**, 017202 (2009).
- ⁴⁶ H. R. Krishna-murthy, K. G. Wilson, and J. W. Wilkins, *Phys. Rev. Lett.* **35**, 1101 (1975).
- ⁴⁷ G. Kotliar and A. E. Ruckenstein, *Phys. Rev. Lett.* **57**, 1362 (1986).
- ⁴⁸ S. Y. Savrasov, V. Oudovenko, K. Haule, D. Villani, and G. Kotliar, *Phys. Rev. B* **71**, 115117 (2005).
- ⁴⁹ M. Gutzwiller, *Phys. Rev.* **134**, A923 (1964).
- ⁵⁰ J. Hubbard, *Proc. Roy. Soc. (London)* A281, 401 (1964).
- ⁵¹ H. Hegger, C. Petrovic, E. G. Moshopoulou, M. F. Hundley, J. L. Sarrao, Z. Fisk, and J. D. Thompson, *Phys. Rev. Lett.* **84**, 4986 (2000).